

Multiple phase transitions in rare earth $\text{RE}_5\text{T}_4\text{M}_{10}$ (T = Rh, Ir and M = Si, Ge, Sn)

S. Ramakrishnan

Department of Condensed Matter and Material Science, Tata Institute for Fundamental Research, Homi Bhabha Road, Mumbai 400 005, India

Rare earth compounds of the type $\text{RE}_5\text{T}_4\text{M}_{10}$ (T = Rh, Ir and M = Si, Ge, Sn) display a variety of phase transitions ranging from charge density wave (CDW), local moment magnetism, antiferromagnetism in the heavy fermion state, superconductivity and giant positive magnetoresistance. In particular, $\text{RE}_5\text{Ir}_4\text{Si}_{10}$ (RE = Dy-Lu) compounds exhibit strong coupling CDW at high temperatures and superconductivity or magnetic ordering at low temperatures, while $\text{RE}_5\text{Rh}_4\text{Ge}_{10}$ (RE = Gd-Tm) show multiple magnetic transitions with large magnetoresistance below the magnetic transitions. Finally, the light rare earth series $\text{RE}_5\text{T}_4\text{Sn}_{10}$ (RE = Ce, Pr, Nd, T = Rh, Ir) display heavy fermion behaviour (for Ce and Pr) and giant positive magneto resistance (for Nd) at low temperatures.

STUDY of multiple phase transitions is one of the frontier areas of condensed matter physics. Large number of investigations were made to understand the magnetism, superconductivity, giant magnetoresistance and charge density wave ordering in both inorganic and organic compounds. Many of them have low dimensional (1D and 2D) structures. The low dimensionality of these compounds is central to the unusual ground states exhibited by these compounds. However, in order to probe them further and search for novel phase transitions, especially those involving the interplay of charge density wave (CDW) with magnetism or superconductivity, new classes of materials are needed.

Our quest for such materials has yielded a series of compounds of the type $\text{R}_5\text{Ir}_4\text{Si}_{10}$ (R = Dy-Lu and Y)¹. In particular, a high quality single crystal of $\text{Lu}_5\text{Ir}_4\text{Si}_{10}$ shows formation of a commensurate CDW along the *c*-axis below 80 K in the (*h*, 0, *l*) plane that coexists with BCS type superconductivity² below 3.9 K. However, in a single crystal of $\text{Er}_5\text{Ir}_4\text{Si}_{10}$, one observes the development of a 1D-incommensurate CDW at 155 K, which then locks into a purely commensurate state below 55 K. The positions of these super lattice reflections can be described by modulation wave vectors $q_1 = (0, 0, 1/4 - \mathbf{d})$, $q_2 = (0, 0, 1/4 + \mathbf{d})$ and $q_3 = (0, 0, 1/2)$. Further, the development of the incommensurate peaks beginning at 155 K are found to merge into a commensurate $q = (0, 0, 1/4)$ single peak³ at 55 K. The well localized Er^{3+} moments are antiferromagnetically ordered below 2.8 K which results in the coexistence of strongly

coupled CDW with local moment antiferromagnetism in $\text{Er}_5\text{Ir}_4\text{Si}_{10}$. Unlike conventional CDW systems, the extremely sharp transition (width ~1 K) in all bulk properties along with huge heat capacity anomalies in these compounds makes this CDW transition an interesting one.

Further, studies on $\text{Gd}_5\text{Rh}_4\text{Ge}_{10}$ revealed quadruple transitions while $\text{RE}_5\text{T}_4\text{Sn}_{10}$ (RE = Ce and Pr) exhibit heavy fermion behaviour at low temperatures. A single crystal of $\text{Nd}_5\text{Rh}_4\text{Sn}_{10}$ showed giant positive magnetoresistance (~100%) below the antiferromagnetic ordering of Nd^{3+} moments.

Experimental

Single crystals of some of the compounds have been grown by the Czochralski method. Crystals of typical size 10 mm long and 3 mm diameter could be grown, the largest surface being perpendicular to the (001) direction. Powder X-ray diffraction confirmed the structure and absence of impurity phases and sharp Laue back scattering pictures showed that the crystals were of high quality.

Results and discussion

Figure 1 shows the crystal structure of $\text{RE}_5\text{Ir}_4\text{Si}_{10}$. This series adopt tetragonal structure (PM3M) and the rare earth has three sites including a chain site along the *c*-axis.

We now present data which establish existence of CDW transition in $\text{Lu}_5\text{Ir}_4\text{Si}_{10}$ below 80 K and its coexistence with bulk BCS type superconductivity below 3.9 K. The resistivity (ρ) shows a transition at 80 K as shown in Figure 2. Similar behaviour is observed in $c(T)$ (lower panel in Figure 2). Both of them show sharp discontinuities (width ~1.0 K) at 80 K (T_{cdw}) with small anisotropy. ρ exhibits normal linear *T* dependence above T_{cdw} but jumps to a higher value below T_{cdw} signifying the opening of a gap in the Fermi surface (FS). Similarly, the drop of *c* at T_{cdw} implies loss in Pauli spin susceptibility due to CDW ordering. The rise in *c* at low temperatures is due to the influence of magnetic impurities at the ppm level in Lu. Figure 3 shows the heat capacity (C_p) data between 2 and 100 K. Heat capacity C_p shows a huge but a sharp peak at T_{CDW} ($\Delta C_p = 160 \text{ J/mol K}$). To the best of our knowledge, such a narrow and huge anomaly in C_p has not been seen in any CDW system including canonical CDW examples such as, NbSe_3 or NbSe_2 . The entropy involved in the CDW

e-mail: ramky@tifr.res.in

transition in $\text{Lu}_5\text{Ir}_4\text{Si}_{10}$ crystal is estimated to be $0.6R$, where R is the universal gas constant ($R = 8.314 \text{ J/mol K}$). The magnitude of the latent heat associated with this transition could not be observed in our experiment which could be either due to the low resolution ($\sim 1\%$) of our heat capacity set up or absence of any latent heat. At low temperatures, we observe another jump in C_p (at 3.9 K) (lower panel in Figure 3) which confirms bulk (BCS) weak coupling superconductivity and this is in agreement with resistivity and susceptibility data. Below 3.5 K , the C_p data could be fitted to a standard BCS expression and the energy gap Δ is estimated to be around 7 K with the electron-phonon coupling constant I equal to 0.43 . Clearly, this indicates $\text{Lu}_5\text{Ir}_4\text{Si}_{10}$ is a simple BCS superconductor which coexists with CDW ordering below 3.9 K . A strong justification for CDW would be the observation of super lattice structure below the transition. Such a structure is indeed observed using single crystal X-ray diffraction and the top panel shows the temperature dependence of the of the fundamental peak $(0, 0, 6)$ and the bottom panel displays super lattice peak $(0, 0, 5 + 3/7)$ from 2 to 100 K in Figure 4.

The super lattice peaks are observed along c -axis below 80 K in the $(h, 0, l)$ plane. They can be indexed as $(h, 0, l+q)$, where $q = m/7$ and $m = 1, 2, 3, 4, 5, 6$. This implies a commensurate lattice structure with seven unit cell period along c -axis. Although the fundamental period of modu-

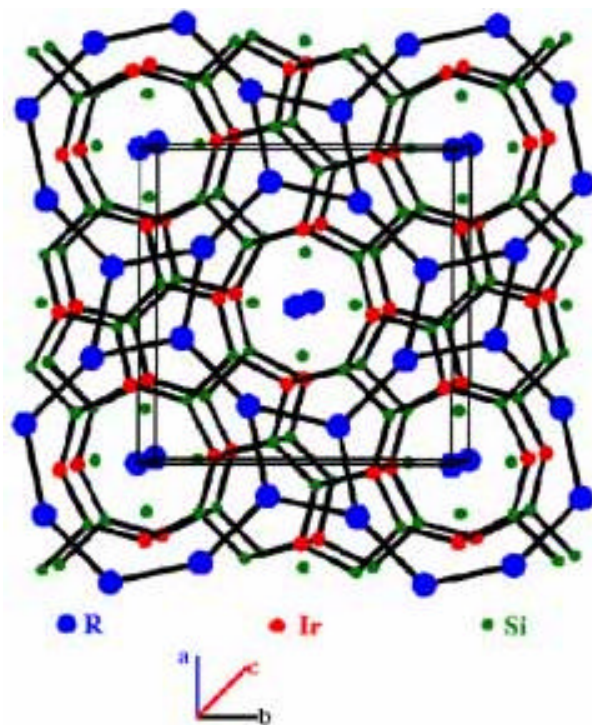


Figure 1. Projection of the crystal structure of $\text{Lu}_5\text{Ir}_4\text{Si}_{10}$ along the $(0, 0, 1)$ direction. Note that there is no direct Ir–Ir contact. C -axis is perpendicular to the plane.

lation seems to be $q = 3/7$, the actual structural modulation is not a simple sine wave because of the presence of higher harmonics. Details of this analysis will be published elsewhere. The presence of the super lattice peak down to 2 K reaffirms the coexistence of CDW ordering with superconductivity in $\text{Lu}_5\text{Ir}_4\text{Si}_{10}$ below 3.9 K . However, in the case of a high quality single crystal of $\text{Er}_5\text{Ir}_4\text{Si}_{10}$, we first observe a combined commensurate structural transition and an incommensurate CDW (155 K), that locks into a purely commensurate state at lower temperatures (55 K), and local moment antiferromagnetism (below 2.8 K). This compound is iso-structural to $\text{Lu}_5\text{Ir}_4\text{Si}_{10}$. As opposed to earlier canonical CDW systems (such as NbSe_3 and NbSe_2), the anomalies of the bulk properties at the 155 K CDW transition are much sharper in $\text{Er}_5\text{Ir}_4\text{Si}_{10}$ and $\text{Lu}_5\text{Ir}_4\text{Si}_{10}$. Thus, we believe that $\text{Er}_5\text{Ir}_4\text{Si}_{10}$ provides a unique opportunity to study local moment magnetism, strongly coupled CDW and their interplay in the same compound. Figure 5 shows the temperature dependence of the resistivity between 1.8 K and 300 K along the a and c -axes. An abrupt increase in r is observed at 155 K which, upon further

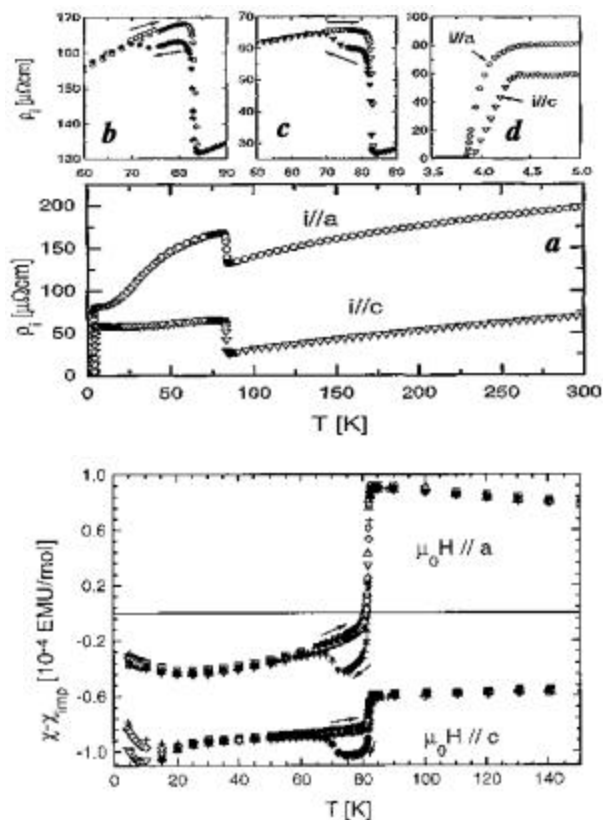


Figure 2. Temperature dependence of resistivity (top panel) and susceptibility (bottom panel) of $\text{Lu}_5\text{Ir}_4\text{Si}_{10}$ along a and c -axes. The top panel insets b) and c) show r behaviour near CDW transition while inset d) shows r near superconducting transition. The bottom panel shows c dependence near the CDW transition. Note the hysteresis in both r and c near the CDW transition.

cooling, develops into a plateau and drops sharply around 55 K. The dramatic changes in $r(T)$ clearly elucidate the presence of two transitions at 155 K and 55 K. The pronounced hysteresis observed between 40 K and 120 K establishes the first order character of the 55 K transition. Note that the anisotropy in resistivity ratio is quite small (2.4). This ratio is indeed much less than that observed in canonical CDW systems, such as NbSe_3 . Low anisotropy indicates strong inter-chain coupling. The behaviour of $r(T)$ could be understood in terms of two conducting channels, one related to the Er1 sites and the other due to the Er2–Er3 network. The first channel undergoes a metal–insulator transition at 155 K while the networks have finite conductivity that remains at all temperatures. Below the lock-in transition ($T=55$ K), the commensurate modulation destroys the perfect nesting and r suddenly drops at this temperature. The magnetic susceptibility $c(T)$ obeys a simple Curie–Weiss law from 20 K to 300 K with an effective local moment $m_{\text{eff}}=9.7m_B$ and a Curie–Weiss temperature $\theta_p=3.0$ K (data not shown). The inset in Figure 5 shows the resistivity anomaly at the magnetic transition at 2.8 K. No anomaly is found at the temperatures of the CDW transitions unlike in the case of $\text{Lu}_5\text{Ir}_4\text{Si}_{10}$. This is explained by the large local moment contribution to the susceptibility, that overwhelms any changes in the Pauli paramagnetism, as were observed in $\text{Lu}_5\text{Ir}_4\text{Si}_{10}$. The low temperature susceptibility data exhibit a peak at 2.8 K, thereby establishing the antiferromagnetic ordering of Er^{3+} moments

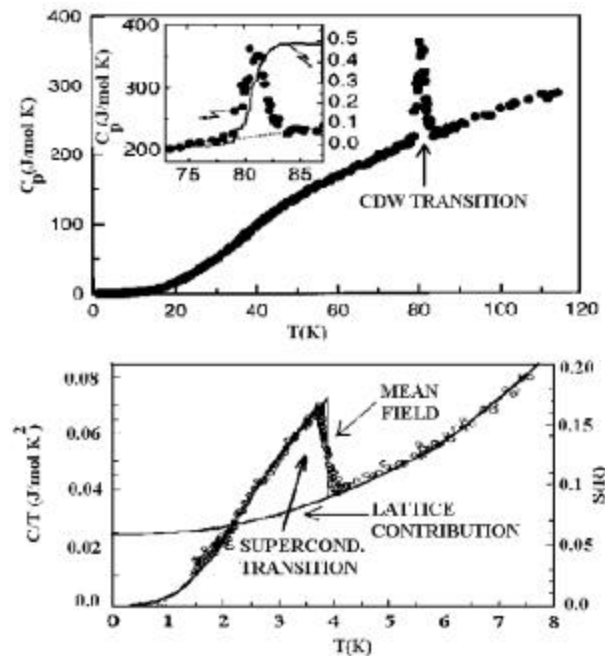


Figure 3. High temperature (top panel) and low temperature (bottom panel) heat capacity (C_p) of $\text{Lu}_5\text{Ir}_4\text{Si}_{10}$. The inset in the top panel shows C_p near the CDW transition and the solid line is the entropy across the transition. The bottom panel clearly shows bulk superconductivity.

below this temperature. Figure 6 presents the specific heat data between 2 K and 160 K of the same crystal.

A huge peak in the specific heat ($\Delta C_p = 160$ J/mol K) is observed at 150 K (see upper insert of Figure 6) while no anomaly is found at the lower transition (55 K). The sharp change ($\Delta T/T_{\text{CDW}} \sim 3\%$) at the upper transition is accompanied by a large entropy change of $0.6R$, where R is the gas constant. This suggests strong electron–phonon coupling in this phase transition which could arise due to a contribution from phonon softening that results in a Kohn anomaly. In our earlier work we have established the occurrence of such a strong coupling CDW in the iso-structural $\text{Lu}_5\text{Ir}_4\text{Si}_{10}$, where the gap is estimated to be around 700 K indicating that the actual phase transition is suppressed well below the mean field value. A similar scenario could also be expected to happen in $\text{Er}_5\text{Ir}_4\text{Si}_{10}$. The bottom inset shows a sharp ($\Delta C_p = 10$ J/mol K) specific heat anomaly at 2.8 K, reflects the bulk nature of the antiferromagnetic magnetic transition of Er moments. Figure 7 shows the super lattice reflection observed as a function of temperature. The twin incommensurate peaks collapse into a single commensurate peak below 55 K.

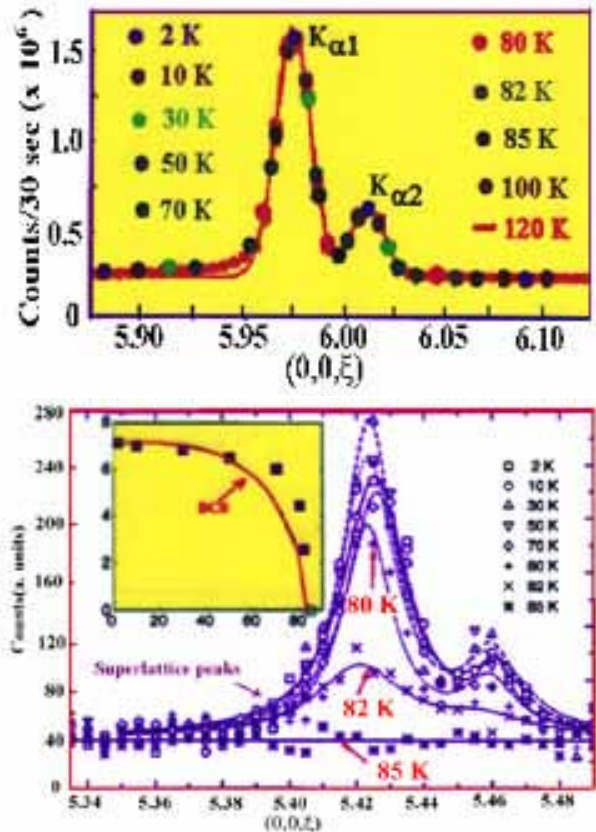


Figure 4. Lattice structural peaks (top panel) and super lattice structural peaks (bottom panel) of $\text{Lu}_5\text{Ir}_4\text{Si}_{10}$. The inset in the bottom panel shows the temperature dependence of the intensity of the super lattice peak which is related to the order parameter of the CDW. The weak coupling BCS dependence is also shown in the same inset.

Figure 8 shows the ‘incommensurability’ d which depends continuously on the temperature and, thus, indicates a truly incommensurate CDW state. At 55 K a lock-in transition

is observed, whereby d jumps to zero, and a 4-fold superstructure results. The lock-in transition is seen as a small increase of the intensity of the $(0, 0, 1/2)$ satellite, as shown in the upper plot of Figure 8. Furthermore, the intensity of the $(0, 0, 1/4)$ satellite ($d=0$), as found from the Q -scan experiment, just below lock-in transition is approximately

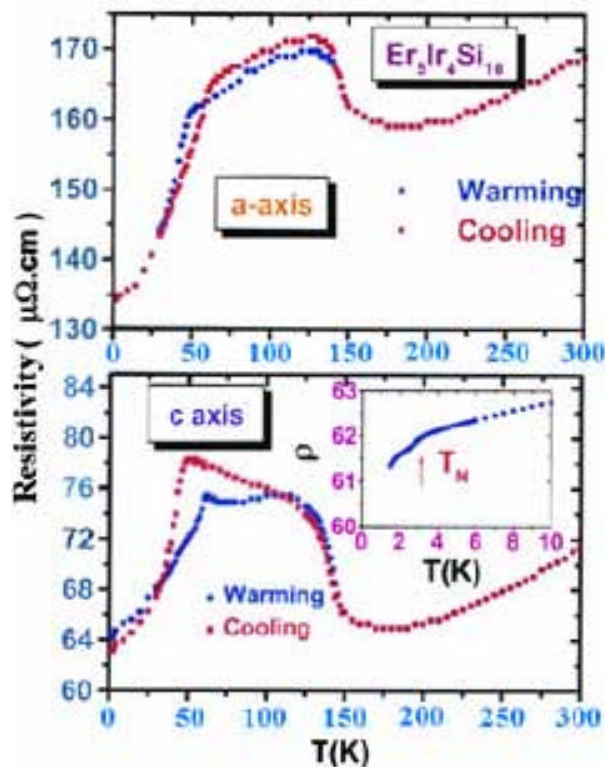


Figure 5. Temperature dependence of resistivity (r) of $\text{Er}_5\text{Ir}_4\text{Si}_{10}$ along a and c -axes. The inset in the lower panel shows the shape of slope of r at low temperatures due to magnetic order of Er moments at 2.8 K.

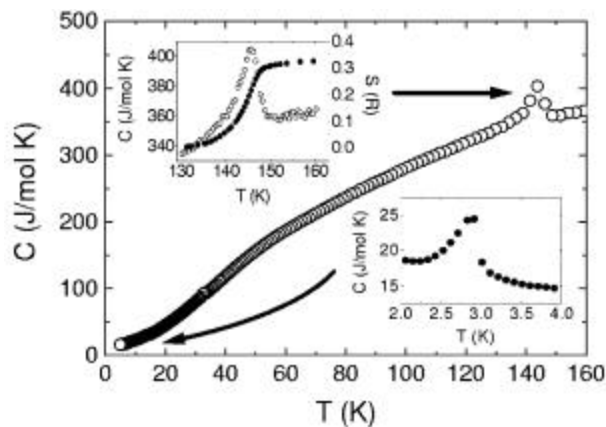


Figure 6. Temperature dependence of the heat capacity (C_p) of $\text{Er}_5\text{Ir}_4\text{Si}_{10}$. The top inset shows C_p near the CDW transition while the bottom inset shows the bulk antiferromagnetic transition at 2.8 K. The solid line in the top inset shows the entropy change across the CDW transition.

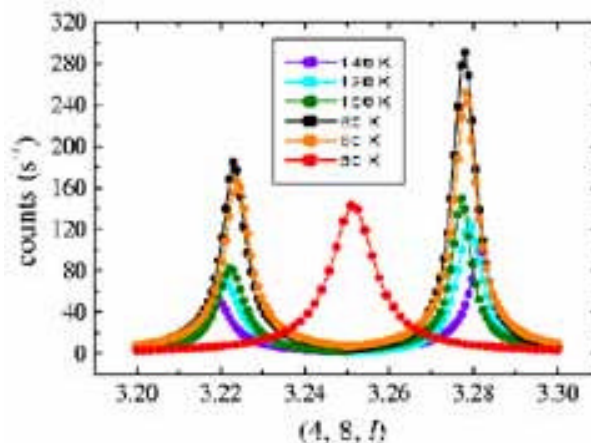


Figure 7. Superlattice reflections of $\text{Er}_5\text{Ir}_4\text{Si}_{10}$ at various temperatures. The incommensurate peaks collapse into a commensurate peak at 50 K.

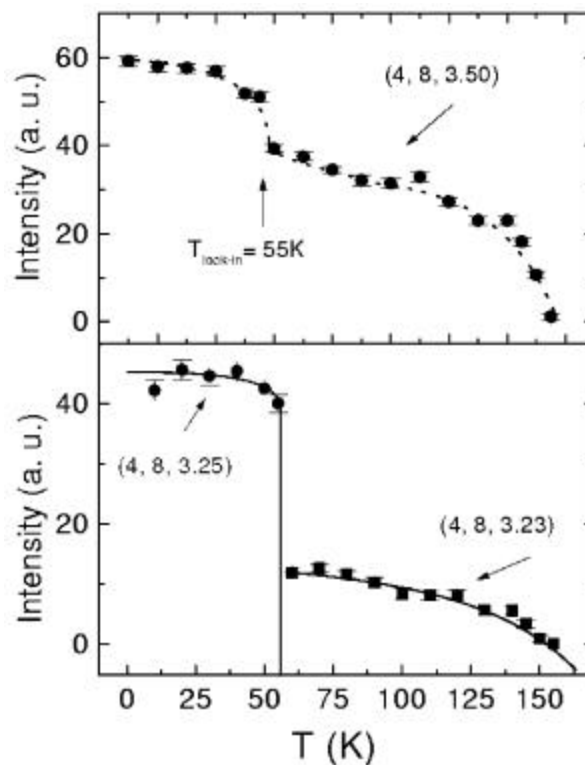


Figure 8. Commensurate and incommensurate charge density wave transitions of $\text{Er}_5\text{Ir}_4\text{Si}_{10}$.

equal to the sum of the intensities of the corresponding incommensurate satellites at $(0, 0, 1/4)$ just above lock-in transition. The simultaneous development of incommen-

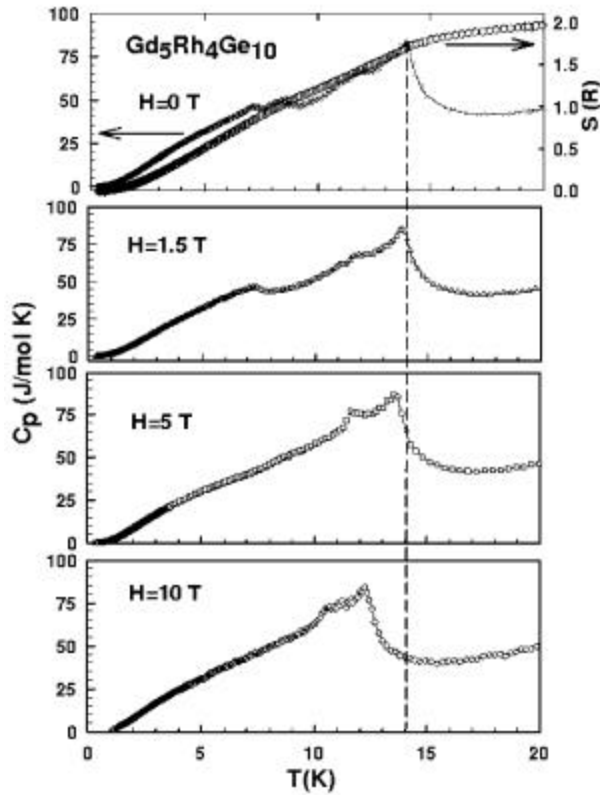


Figure 9. Heat capacity of $\text{Gd}_5\text{Rh}_4\text{Ge}_{10}$ at various magnetic fields. The dotted line shows the transition in 0 field.

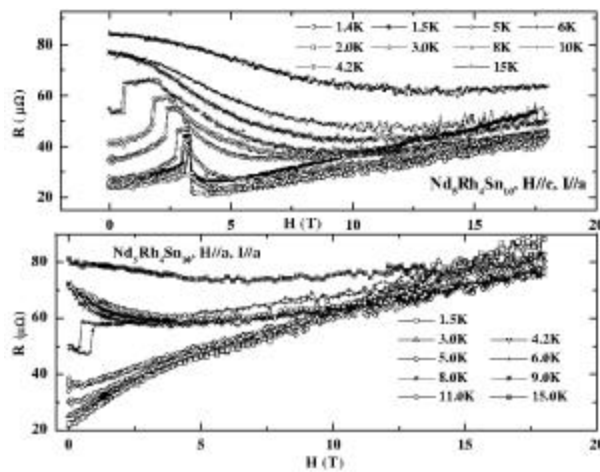


Figure 10. Magnetoresistance of $\text{Nd}_5\text{Rh}_4\text{Sn}_{10}$ along a and c -axes. The top panel is transverse magnetoresistance and the bottom panel is longitudinal magnetoresistance. The sharp change at low fields below 6 K is due to the metamagnetic transition.

surate and commensurate modulations makes the $\text{Er}_5\text{Ir}_4\text{Si}_{10}$ an atypical CDW system. Two scenarios can be envisaged to explain this feature. In the first, it is assumed that at T_{CDW} the unit-cell doubles. The Fermi-surface is modified accordingly and allows nesting resulting in a 1D-incommensurate CDW, where $q_{1\text{D}} = (0, 0, 1/2 - 2d)$ with respect to the doubled unit-cell. We note that a transition towards a structure with a doubled c -axis is possible via a second-order phase transition. Therefore, we propose that the transition at $T_{\text{CDW}} = 155$ K, is a second-order, structural phase transition. The modified electronic structure could then induce the CDW transition, whereby the order parameter of the CDW grows in concert with the order parameter of the structural transition. The CDW state might be favoured in the doubled unit cell by a better nesting condition or by an increased electron-phonon coupling. Polycrystalline and single crystal neutron data suggest⁴ the presence of a large magnetic moment on the Er1 site and smaller ones on Er2 and Er3 sites, below 2.8 K. The presence and interaction of local moments in this material classify $\text{Er}_5\text{Ir}_4\text{Si}_{10}$ as the first intermetallic CDW system with local moment ordering. Although it is possible to understand the behaviours of r and c within the CDW and local moment pictures, the large peak in the C_p at 145 K denotes this CDW transition as an unusual one, unlike conventional CDW systems where the anomalies in the bulk properties are quite weak at the transition. It is generally believed that defects tend to wipe out the sharp anomaly in conventional CDW compounds. In stoichiometric single crystal $\text{Er}_5\text{Ir}_4\text{Si}_{10}$, we expect that the influence of defects will be much smaller making this system essentially disorder free. One does not observe any anomaly in C_p around 55 K since it is a lock-in transition, which probably involves very small entropy change but a large change in the resistivity due to the decrease of the energy gap. In conclusion, we have established that $\text{Er}_5\text{Ir}_4\text{Si}_{10}$ exhibits multiple

Table 1. Comparison of CDW systems. $\text{RE}_5\text{Ir}_4\text{Si}_{10}$ offers clean and sharp CDW among all systems

Compound	T_{CDW} (K)	$\Delta T/T_{\text{CDW}}$ (%)	ΔS (R)
TTF-TCNQ	54	20	~0.03
NbSe ₃	145	4.8	~0.01
	58	1.7	~0.005
K _{0.3} MoO ₃	180	7	~0.11
Li _{0.9} Mo ₆ O ₁₇	24	25	~0.03
K _{0.0} Mo ₆ O ₁₇	120	20	~0.03
Tl _{0.9} Mo ₆ O ₁₇	113	18	~0.038
<i>h</i> -Mo ₄ O ₁₁	30	8	~0.004
	109	14	~0.07
<i>g</i> -Mo ₄ O ₁₁	113	–	–
Lu ₅ Ir ₄ Si ₁₀	83	1	~0.5
Er ₅ Ir ₄ Si ₁₀	155	2	~0.6
	55	–	–
Tm ₅ Ir ₄ Si ₁₀	135	2	~0.8
	120	–	–
	~17 K?	–	–

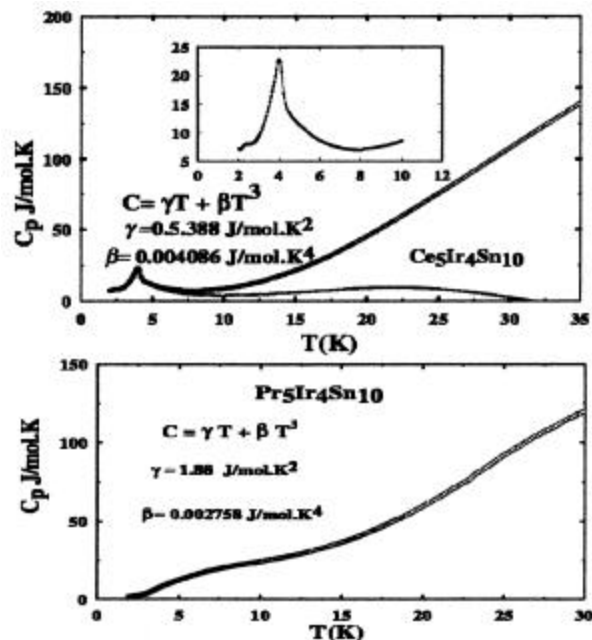


Figure 11. Temperature dependence of heat capacity (C_p) $Ce_5Ir_4Sn_{10}$ and $Pr_5Ir_4Sn_{10}$. Inset in the top panel shows antiferromagnetic ordering Ce moments at 4 K.

CDW transitions (1D-incommensurate at 155 K and lock-in at 55 K) and a transition towards a magnetically ordered state at 2.8 K. We speculate that the magnetic moments of the Er atoms play a definite role in these transitions and further understanding requires band structure calculations to determine the possible nesting and gapping of the Fermi surface which leads to the CDW transitions. It is worthwhile to compare $R_5Ir_4Si_{10}$ with the other canonical CDW systems in Table 1. One clearly sees that $R_5Ir_4Si_{10}$ compounds display much sharper CDW transitions with large entropies associated with such transitions. We stress that the present series offer a new and extremely convenient paradigm with which to study strong coupling CDW and coexisting superconductivity or magnetism. We now present⁵ the unusual multiple magnetic transitions observed in $Gd_5Rh_4Ge_{10}$ where there is no crystal-field contribution. Figure 9 shows the heat capacity data that displays quad-

ruple magnetic transitions. It appears that one of the four-fold transitions that occurs at the highest temperature is a second-order continuous phase transition while the other three probably involve moment reorientations and non-collinear amplitude modulations. However, only the two transitions that occur at high temperatures survive in the presence of magnetic field. To the best of our knowledge this is the first instance a quadruple transition is seen in a Gd compound. In general, the basic cause of the magnetic orderings is due to anisotropic indirect exchange interaction (Ruderman–Kittel–Kasuya–Yosida) type coupled with multiple site occupancy of the Gd atoms.

Finally, an example of a giant positive magnetoresistance realized in a single crystal⁶ of $Nd_5Rh_4Sn_{10}$ which displays a second order antiferromagnetic transition followed by a first order spin flop transition. The large positive magnetoresistance shown in Figure 10 is attributed to the spin disorder scattering coupled with Nd ions occupying three different sites in this compound.

The light rare earths $Ce_5Ir_4Sn_{10}$ and $Pr_5Ir_4Sn_{10}$ exhibit heavy fermion behaviour with large Sommerfeld coefficients (see Figure 11) with the former undergoing antiferromagnetic ordering⁷ below 10 K. In conclusion we reiterate that unusual multiple phase transitions are realized in the 5–4–10 structure depending on the choice of the elements. One can observe superconductivity and magnetism, coexistence of charge density wave with magnetism or superconductivity, giant magnetoresistance and heavy fermion behaviour in these systems. Band structure calculations to understand the various phase transitions displayed by the 5–4–10 compounds will be extremely rewarding given that high quality single crystal data are already available.

1. For earlier references on polycrystalline work, see *Phys. Rev.*, 1991, **B43**, 7688; *Phys. Rev.*, 1993, **B48**, 4152 and references cited therein.
2. Becker, *et al.*, *Phys. Rev.*, 1999, **B59**, 7266.
3. Galli, F. *et al.*, *Phys. Rev. Lett.*, 2000, **85**, 159.
4. Galli, F. *et al.*, *Phys. Rev.*, 2000, **B62**, 13840.
5. Ramakrishnan, S. *et al.*, *Phys. Rev.*, 2003, **B68**, 94420.
6. Ramakrishnan, S. *et al.*, *Phys. Rev.*, 2001, **B63**, 184402.
7. Patil, N. *et al.*, *Phys. Rev.*, 1997, **B56**, 3360.

ACKNOWLEDGEMENTS. This work was done in collaboration with Prof. J. A. Mydosh and his group at Kamerlingh Onnes Laboratory, Leiden, The Netherlands.